CORROSION SCIENCE AND TECHNOLOGY, Vol.6, No.4(2007), pp.198~205

Binary Compound Formation Upon Copper Dissolution: STM and SXPS Results

N.T.M. Hai[1], S. Huemann[1], R. Hunger[2], W. Jaegermann[2], P. Broekmann[1,†], and K. Wandelt[1]

[1]Institute of Physical and Theoretical Chemistry, University of Bonn, Wegelerstr. 12, D-53115 Bonn, Germany
[2]Department of Material Science, Technical University of Darmstadt, Petersenstr. 23, 64284 Darmstadt, Germany

The initial stages of electrochemical oxidative CuI film formation on Cu(111), as studied by means of Cyclic Voltammetry (CV), in-situ Scanning Tunneling Microscopy (STM) and ex-situ Synchrotron X-ray Photoemission Spectroscopy (SXPS), indicate a significant acceleration of copper oxidation in the presence of iodide anions in the electrolyte. A surface confined supersaturation with mobile CuI monomers first leads to the formation of a 2D-CuI film via nucleation and growth of a Cu/I-bilayer on-top of a pre-adsorbed iodide monolayer. Structurally, this 2D-CuI film is closely related to the (111) plane of crystalline CuI (zinc blende type). Interestingly, this film causes no significant passivation of the copper surface. In an advanced stage of copper dissolution a transition from the 2D- to a 3D-CuI growth mode can be observed.

Keywords *: copper halides; anodic film formation; in-situ STM; surface phase transitions*

1. Introduction

Copper has become one of the most important materials in modern semiconductor technology due to its nowadays application as on-chip wiring material for state-of-the-art integrated logic devices.[1)-3)] Here, the so called *super-conformal filling* of trenches or vias by copper material is achieved by a sophisticated interplay between various *accelerators* and *suppressors* that are added to the plating bath. Although this so-called Copper Damascene Process is already well established in the current chip technology there is still a tremendous lack of the atomic scale understanding of the relevant interactions between the copper surface and cuprous species on the one hand and the various additives on the other hand.

One of the most serious draw-backs in this technology is the inclusion of halide anions or copper halide salts into the growing copper film which causes considerable conductivity problems especially if the wiring features reach nanometer sizes. Therefore, an investigation of the impact of halide anions on the dissolution or deposition reaction of copper is important, in particular at the open circuit potential and at low overpotentials.

Broekmann et al. recently reported on the reversible growth/dissolution of an ultra-thin 2D-CuI film on an iodide pre-covered Cu(100) electrode at potentials *below* the formation of 3D-CuI clusters.[4)-5)] Quite surprisingly, this 2D-CuI film does not fully suppress copper deposition or dissolution, the copper surface remains reactive.

The present work extends these investigations to the structural characterization of a 2D-CuI film grown on an iodide pre-covered Cu(111) electrode surface. In order to distinguish between the first adsorbed iodide layer, the 2D-CuI film and 3D-CuI clusters we combine in this study cyclovoltammetric (CV) measurements with in-situ STM (Scanning Tunneling Microscopy) and ex-situ SXPS (Synchrotron X-ray Photoemission Spectroscopy).

2. Experimental

The Cu(111) single crystal surface (orientation less than 0.5° off the (111) plane) was etched in 50 % orthophosphoric acid prior to each experiment in order to remove the native oxide film which is formed in air.

All solutions were prepared from high purity water (conductivity < 18 MΩ · cm; TOC < 5 ppb) and reagent grade chemicals, and were routinely deoxygenated with argon several hours before use. All potentials given in the text refer to a RHE reference electrode.

An experiment routinely started with an electrochemical

† Corresponding author: broekman@pc.uni-bonn.de

characterization of the Cu(111) electrode in the pure 5 mM H_2SO_4 which also served as supporting electrolyte for all subsequent measurements in iodide containing solution. For these latter experiments the pure supporting electrolyte was exchanged *under potential control* (E = +50 mV vs. RHE) by a solution of 5 mM H_2SO_4 and 1 mM KI, in order to avoid instantaneous formation of thick 3D-CuI films.

All microscopic experiments have been performed using a home-built EC-STM (Electrochemical Scanning Tunneling Microscope).[6] Ex-situ high resolution photoemission studies with synchrotron radiation were performed at the SoLiAS (Solid/Liquid interface Analysis System) experimental station at the undulator beamline U49/2-PGM2 at BESSY II after an air free transfer of the Cu sample from the electrochemical cell into the vacuum chamber.[7]

3. Results and discussion

3.1 Electrochemical characterization

Fig. 1 displays steady-state CVs (Cyclic Voltammograms) of Cu(111) in both the pure and the iodide containing electrolyte. The black curve contains all typical features of the CV of Cu(111) in 5 mM sulfuric acid solution,[8)-12)] i.e. an extended double layer regime between +260 mV and +100 mV, the exponential increase in the anodic potential sweep due to copper dissolution starting at +260 mV, and a pronounced peak at +285 mV in the reverse potential sweep due to the re-deposition of afore dissolved copper material. The pair of additional current waves (P/P`) correlates with the adsorption (desorption) and the subsequent formation (decay) of a laterally well ordered sulfate/water co-adsorption layer.[8)-14)] The exponential increase of the cathodic current starting at -260 mV after passing P' is due the on-set of the hydrogen evolution reaction (HER).

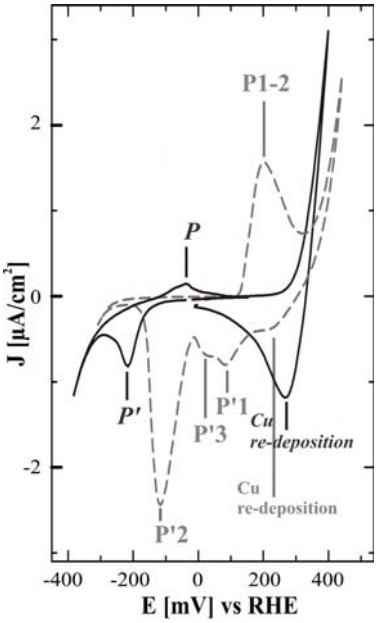

Fig. 1. Cyclic voltammogram of Cu(111) in pure 5 mM H_2SO_4 (black curve) and in 5 mM H_2SO_4/1 mM KI (grey curve), dE/dt = 10 mV/s.

Iodide anions instantaneously remove the sulfate/water co-adsorption layer from the electrode surface after electrolyte exchange (grey dashed curve in Fig. 1). The most striking new feature is an anodic peak system P1-2 centered at about +214 mV as already reported by Irish et al. for polycrystalline copper,[15)] by Inukai et al.[16)] for Cu(111) and by Broekmann et al.[4),5)] for Cu(100) exposed to the same electrolyte as used in the present study. This pronounced anodic current feature was explained in terms of massive CuI formation (solubility product $K_s = 1.2 \cdot 10^{-11.3}$ M^2 l^{-2}) involving electro-oxidation of copper to cuprous Cu^+ species.[4),5),16)]

After passing the peak system P1-2 the anodic current does not drop to zero indicating that the grown CuI film is less effective in passivating the copper electrode against anodic dissolution processes than the $Cu_2O/CuO,Cu(OH)_2$ duplex film which grows on copper in an 0.1 M NaOH electrolyte solution.[17,18] Compared to the blank supporting electrolyte the copper dissolution just shifts by $\Delta E \approx 60$ mV to higher potentials in the presence of CuI.

In the cathodic potential scan several cathodic current waves emerge. The first "bump" at about E = +260 mV has to be assigned to the re-deposition of afore dissolved copper material in the presence of CuI. Relative to the iodide free electrolyte the maximum of this copper re-deposition peak is shifted towards lower potentials by $\Delta E \approx 45$ mV. Compared to the current densities during dissolution in the anodic potential scan this re-deposition peak appears small suggesting that not the entire dissolved material is re-deposited as metallic copper. A plausible explanation for this behavior is the reaction of some dissolved cupric species with iodide anions directly at the surface or in solution to solid CuI followed by 3D-CuI cluster precipitation onto the electrode surface.

Three further cathodic current waves denoted as P'1 (E = +95 mV), P'2 (E = -102 mV) and P'3 (E = +40 mV) evolve at more negative potentials. A similarly complex CV for Cu(100) in iodide containing sulfuric acid has been rationalized in terms of various solid CuI phases which differ in their *structural relation* to the copper electrode. This hypothesis was recently substantiated by in-situ STM studies.[4),5)] Therefore the same explanation is proposed here for the Cu(111)/I system. The peak system P1/P'1

corresponding to the formation/dissolution of the 2D-CuI film shows a much smaller hysteresis than the peak system P2/P'2 indicating the growth/decay of 3D-CuI clusters.

3.2 STM Results

STM images of Cu(111) in blank sulfuric acid solution recorded at sufficiently negative electrode potentials reveal the characteristic surface morphology, namely monoatomically high copper steps with a fringed appearance, and the bare (111) substrate structure on the terraces (Fig. 2a). Passing peak P in the positive potential sweep (Fig. 1) causes the adsorption and subsequent lateral ordering of sulfate/bisulfate anions and co adsorbed water species giving rise to the well known sulfate/water Moiré pattern (Fig. 2b).[8)-14)]

Exchange for the iodide containing electrolyte leads to the instantaneous removal of the sulfate/water co-adsorption phase by a well ordered iodide layer. At low electrode potentials close to the on-set of the HER the iodide anions form a perfect hexagonal $(\sqrt{3}\times\sqrt{3})$R30°-I adlattice with a coverage of $\theta = 0.33$ ML.[19)] Applying higher potentials leads to a uniaxial compression of this adlattice giving rise to the appearance of a striped long-range superstructure superimposed on the atomic scale corrugation (Fig. 2c). *l*, which defines the characteristic distance between adjacent stripes, changes with changing potentials due to an electro-compression/-decompression of the pristine $(\sqrt{3}\times\sqrt{3})$R30° adlattice.[16),19)]

By sweeping the electrode potential from +80 mV to +120 mV we observe more drastic structural changes on the electrode surface (Fig. 3):

Process 1: Local copper dissolution

Fig. 3a reveals the typical morphology of Cu(111) covered with the uniaxially compressed iodide saturation layer (not resolved by STM on this scale). Comparing Fig. 3a and Fig. 3b it becomes evident that the surface is already under reaction reaching P1.[4),5)] Copper steps recede with time according to an inverse step flow mechanism in k Fig. 1.[4),5)] From these results it becomes obvious that iodide facilitates and accelerates the copper oxidation. Note that copper dissolution involving net mass transport into the solution starts in the pure supporting electrolyte only at about E = +280 mV (Fig. 1).

Process 2: 2D-CuI film formation by nucleation and growth on terraces

While in the blank supporting electrolyte highly soluble cupric hex-aquo complexes are formed as final dissolution products the local copper dissolution in the iodide containing electrolyte interferes with a rapid nucleation and growths of a 2D-CuI film (Fig. 3b, c). Copper terraces already covered by the 2D-CuI film are labeled as T1' and T2' while terraces covered by the iodide *adsorption* layer are denoted as T1-T3.

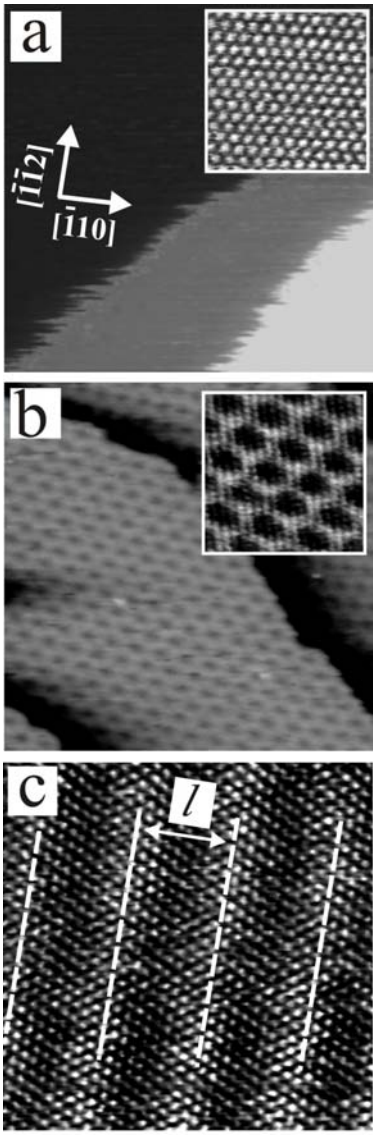

Fig. 2. a) – b) Cu(111) exposed to the pure supporting electrolyte (5 mM H_2SO_4). a) Bare copper surface, 30 nm×30 nm, I_t=1 nA, U_{bias}=20 mV, E_{work}=-210 mV (anodic sweep), the in-set shows an atomically resolved image of the bare copper surface, 3 nm×3 nm, I_t =10 nA, U_{bias} = 5 mV, E_{work} = -210 mV (anodic sweep); b) Sulfate covered copper surface, 40.8 nm×40.8 nm, I_t =5 nA, U_{bias} = 25 mV, E_{work}= +150 mV; the in-set shows the atomic structure of the sulfate covered copper surface, 13.7 nm×13.7 nm, I_t = 5 nA, U_{bias} = 25 mV, E_{work} = +150 mV; c) Electro-compressed iodide adlayer on Cu(111) under saturation conditions, 13.6 nm×13.6 nm, I_t = 3 nA, U_{bias} = 12 mV, E_{work} = +100 mV.

The experimental results can be explained on the basis

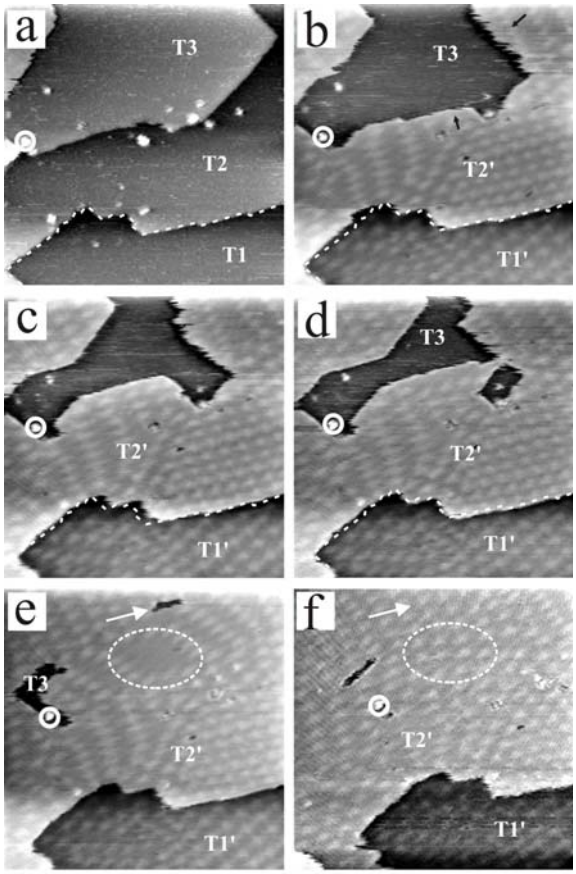

Fig. 3. Growth of a Cu/I-bilayer on the iodide modified Cu(111) electrode, a) – f) 95 nm×95 nm, I_t=0.3 nA, U_{bias}=322 mV, E_{work} = +130 mV. The small white circle marks a stationary feature in all images.

of the following scenario: Depending on the applied potential a stationary equilibrium concentration of cuprous species, probably CuI or $[CuI_2]^-$ monomers,[15),20)] is established. These are diffusing on-top of the anion covered electrode surface. It can be further assumed that the detachment of copper atoms from step edges followed by their complexation with iodide anions represents the first step of copper oxidation. Before reaching the potential range where the 2D-CuI film is formed these diffusing cuprous species are in equilibrium with the step edges. In this sense substrate steps act as "*source*" for a 2D gaseous like phase of CuI or $[CuI_2]^-$ species on terraces. An increase of the electrode potential increases their concentration on terraces until a critical threshold, i.e. the 2D analogue to the solubility product (K_s), is reached. Thus, the solubility product is exceeded (supersaturation) only at the surface giving rise to the *surface confined* nucleation and growth of the 2D-CuI film. The consumption of mobile CuI/$[CuI_2]^-$ monomers by the growing 2D-CuI film disturbs the equilibrium between the steps and the mobile CuI on the terraces. In this sense, the growing 2D-CuI film acts as "sink" for mobile CuI/$[CuI_2]^-$ species. In this initial stage it is not the massive copper dissolution which causes the nucleation and growth of CuI at the surface.[4),5)] Apparently, it is the nucleation and growth of the 2D-CuI film itself that consumes copper material and thereby accelerates the dissolution of copper material from step edges at these low potentials. In this initial stage of the 2D-CuI film formation there is a clear spatial separation between copper oxidation and complexation by the iodide anions at step edges and the nucleation of 2D-CuI film on terraces.

Process 3: Direct conversion of substrate terraces into the 2D-CuI film

Another reaction pathway becomes dominant in an advanced stage of the 2D-CuI film growth, in particular when the fast growing 2D-CuI film reaches a lower step edge that belongs to a substrate terrace which itself is not yet covered by the 2D-CuI film. Terrace T2' in Fig. 3 represents the former substrate terrace T2 which is now covered by the 2D-CuI film. Once T2' reaches the lower step edge of T3 (already seen in Fig. 3b), the 2D-CuI film growth does not come to a standstill at that point. Terrace T3 shrinks with time. In fact, the 2D-CuI film growth continues, but now with a significant slower growth rate than before. In this advanced stage of 2D-CuI film formation there is no more significant spatial separation between copper oxidation and the 2D-CuI film formation. Concerted copper oxidation and 2D-CuI formation takes place directly at the border line between the substrate terrace T3 and the growing 2D-CuI film at T2'.

It should be noted that not the entire copper material from terrace T2 is consumed by the growing 2D-CuI film since the concentration of cuprous ions within the 2D-CuI film is significantly lower than in the copper terrace as it will be argued below. Hence, some extra material has to be expelled onto the receding terrace T2, most likely also in form of mobile CuI or $[CuI_2]^-$ species.

Process 4: Ripening of the 2D-CuI film

Post-growth ripening processes lead to a significant decrease of the pit density with time (see white arrows in Fig. 3e-f). Also the atomic scale ordering within the 2D-CuI film is strongly affected by these post growth ripening processes (see white circles in Fig. 3e-f).

Fig. 4 summarizes all results of the time-resolved STM experiment. Both growth modes of the 2D-CuI film differ not only in their kinetics but also in their final film morphology. Typically, the nucleation and growth mode (process 2 in Fig. 4b-c) produces step edges (type-A) that simply reflect the single Cu-Cu interlayer spacing of

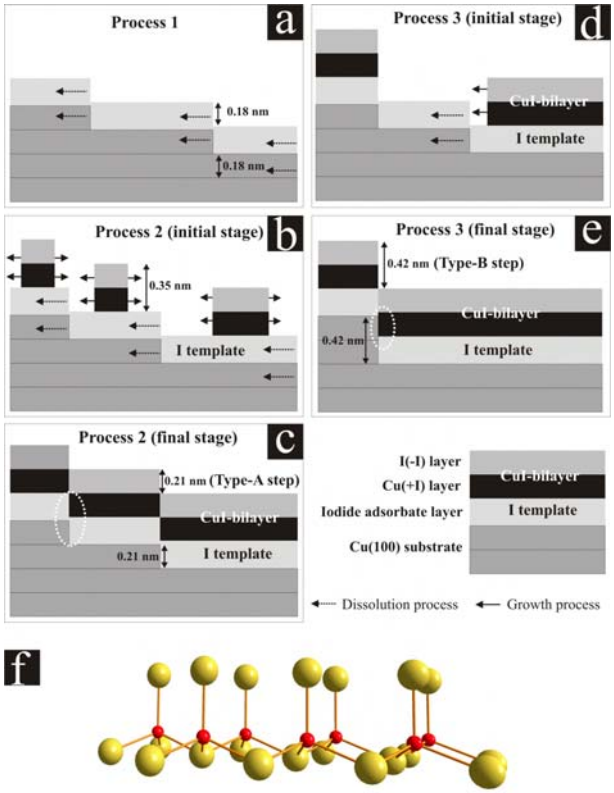

Fig. 4. a) – e) Schematic drawings demonstrating the two reaction pathways leading to the formation of the 2D-CuI film. a) Process 1: Copper dissolution reaction in the presence of the iodide adsorption layer; b) – c) Process 2: Nucleation and growth of the Cu/I-bilayer on iodide covered copper terraces; d) – e) Process 3: Direct transformation of copper terraces into the 2D-CuI film; f) 2D-cut through the CuI_{bulk} lattice parallel to the (111), lane.

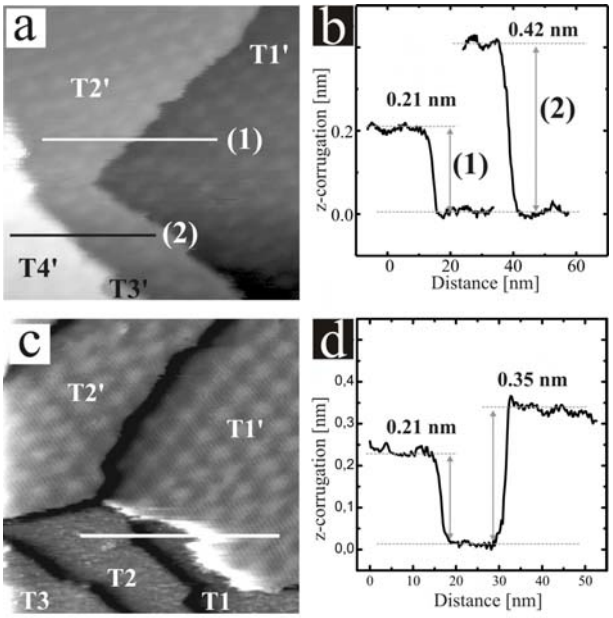

Fig. 5. Morphological aspects of the electrode in the presence of the Cu/I-bilayer, a) 68 nm×68 nm, 68 nm×68 nm, I_t = 5 nA, U_{bias} = 86 mV, E_{work} = +117 mV; b) Cross sections along the white and black line in a); c) 68 nm×68 nm, I_t = 0.14 nA, U_{bias} = 68 mV, E_{work}= +92 mV (cathodic potential sweep); d) Cross section along the white line in c).

$d_{(type\text{-}A)}$ = 2.1 Å. However, apart from that we should also find step edges (type-B) with the double Cu-Cu interlayer separation of $d_{(type\text{-}B)}$ = 4.2 Å as the result of the direct conversion of terraces into the 2D-CuI film (process 3) as indicated by figs. 4d-e. Locally, process 3 can even lead to a smoothening of the electrode surface since the step edge density decreases as a result of a complete terrace etching in the course of the 2D-CuI film formation (see Fig. 3).

An experimental differentiation between the different growth modes and stages can be made by measuring step heights. Fig. 5b shows height profiles along the white and black line in Fig. 5a. The two observed step heights of 0.21 nm and 0.42 nm between T'2 vs. T'1 (single step height) and T'4 vs. T'2 (double step height) support the growth modes proposed in Fig. 4.

The growth and the dissolution of the 2D-CuI film can be understood only on the base of lateral and surface confined diffusion of CuI/$[CuI_2]^-$ species. A mass transport through the electrolyte phase is not needed in order to explain the observed growth and dissolution processes.

The exact height of the 2D-CuI film is determined by cross section d in Fig. 5 in the submonolayer regime with d_{CuI}=3.5±0.15 Å (see also Fig. 5c). This value is in excellent agreement with the iodide interlayer spacing along the [111] direction in crystalline CuI with $d_{CuI(111)}$=3.5 Å. Fig. 4f displays a cut through the crystalline structure of bulk CuI (zinc blende type) parallel to the (111)-plane including one central layer of cuprous ions that is "sandwiched" by two iodide layers. The same stacking sequence is assumed for the 2D-CuI film on Cu(111) with the lower iodide layer being in direct contact to the copper substrate. This lower iodide adlayer can be identified with the pre-existing iodide adsorbate layer. From that point of view we can understand the 2D-CuI film formation as the growth of a Cu/I-bilayer on-top of the pre-exiting iodide adsorbate layer resulting in the I/Cu/I-trilayer. In this simple picture the specifically adsorbed iodide does not chemically "react" with cuprous CuI/$[CuI_2]^-$ species, but serves as a *template* layer for the Cu/I-bilayer formation atop. All dynamics (growth, decay, ripening) as observed in the STM solely affect the Cu/I-bilayer on-top of the iodide adsorption layer. This hypothesis will be substantiated in the next section by means of high-resolution photoemission experiments.

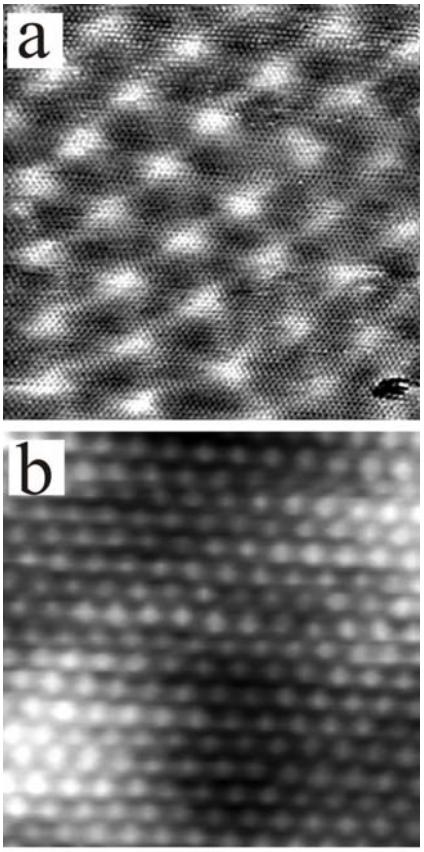

Fig. 6. Atomic scale structure of the 2D-CuI film on Cu(111), a) Pseudo-hexagonal long-range height modulation of the 2D-CuI film, 27 nm×27 nm, I_t = 4.5 nA, U_{bias} = 372 mV, E_{work} = +125 mV; b) Dislocations within the Cu/I-bilayer (note wavy rows of atoms), 5.2 nm×5.2 nm, I_t = 4.5 nA, U_{bias} = 372 mV, E_{work} = +125 mV.

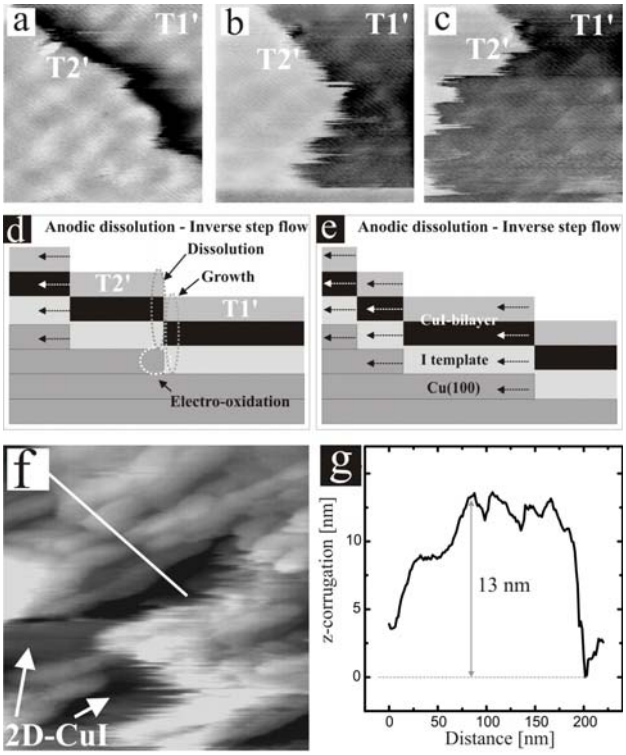

Fig. 7. Copper dissolution in the presence of the 2D-CuI film, a) – c) 27 nm × 27 nm, I_t = 1 nA, U_{bias} = 112 mV, E_{work} = +127 mV; d) – e) Schematic drawing illustrating the inverse step flow mechanism in the presence of the 2D-CuI film; f) Appearance of 3D-CuI cluster as final products of the anodic copper dissolution, 293 nm×293 nm, I_t = 0.1 nA, U_{bias} = 433 mV, E_{work} = +120 mV (note that the CuI clusters have been formed upon passing anodic peak system P1-2 in Fig. 1); g) Cross section along to the white line in f).

Note that the Cu/I-bilayer undergoes a ripening process just after the initial growth leading to a significant improvement of the lateral order. On the atomic scale the Cu/I-bilayer reveals an almost hexagonal arrangement of STM dots (Figs. 6a b) which are assigned to the terminating iodide of the Cu/I-bilayer. Similar to the Cu/I-bilayer film recently found on Cu(100) under UHV[21] and electrochemical conditions[4),5)] we determine a Nearest Neighbor Distance on Cu(111) of NND = 0.41 nm±0.03 nm that is quite similar to the interatomic spacings of iodide and cuprous ions within the (111) plane of bulk CuI with NND_{CuI}=0.4287 nm.

The 2D-CuI film can be stabilized only within a narrow potential window ranging from about +100 mV to +125 mV. A further increase of the electrode potential to E_{work} = 127 mV leads to the restart of copper dissolution but now in the presence of the covering 2D-CuI film that obviously does not act as an effective passivation layer. Fig. 7a-c presents a series of STM images showing the receding of terraces according to an "inverse step flow" mechanism. Characteristically, the 2D-CuI film with the typical long-range Moiré modulation (see Fig. 6) appears on terrace T1' upon receding of terrace T2'. Considering the proposed stacking sequence of the 2D-CuI film it becomes obvious that at least 4 atomic layers must be involved into the dissolution reaction as indicated in Figs. 7d-e, namely the topmost metallic copper layer, the iodide adsorption layer (I template) and the Cu/I-bilayer as well.

Copper material dissolved by this process nucleates and grows in form of 3D-CuI clusters (Fig. 7f-g). However, it is not clear yet whether the 3D-CuI clusters nucleate directly on-top of the 2D-CuI film or in solution followed by their precipitation onto the 2D-CuI film.

3.3 Electron spectroscopy

In order to complement our in-situ STM data with a chemically sensitive probe we performed ex situ XPS measurements at the synchrotron X-ray source BESSY II.

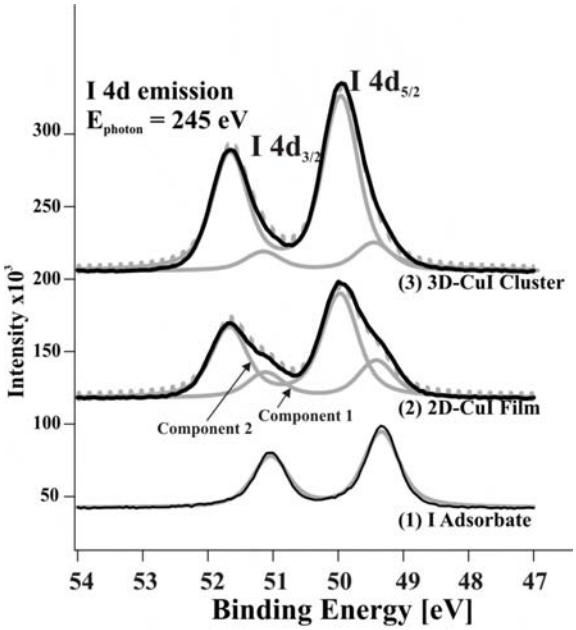

Fig. 8. a) I4d emission obtained at E_{photon} = 245 eV, (black curve: original XPS spectrum, grey curves: fitted curves, grey dotted line: sum of fitted curves).

Therefore, copper samples were transferred from the electrochemical environment into the UHV by emersion of the electrode out of the electrolyte at three particular potentials being characteristic for the presence of (1) the iodide adsorbate ($E_{emersion}$ = -100 mV), (2) the 2D-CuI film ($E_{emersion}$ = +125 mV) and (3) the 3D-CuI clusters ($E_{emersion}$ = +175 mV). Note, in the latter case the anodic peak system P1-2 has been passed in the anodic potential scan in order to produce the 3D-CuI clusters before the sample was emersed out of the electrolyte at $E_{emersion}$ = +175 mV in the reverse scan. Excitation energies of E_{photon} = 1040 eV, E_{photon} = 720 eV and E_{photon} = 245 eV were used for the systematic variation of the escape depth of photoelectrons thereby tuning the surface sensitivity in the photoemission experiment. Exemplarily, we present spectra of the three surface states of interest obtained with an excitation energy of E_{photon} = 245 eV.

Our main interest is focused on the question whether the pre-adsorbed iodide phase remains intact upon the Cu/I-bilayer growth atop as concluded from the STM experiments. I (4d) photoemission from all three surface states of interest (Fig. 8a), i.e. the I adsorbate layer, the 2D-CuI film, and the 3D-CuI clusters. The key information we can draw from this experiment is that the I (4d) spectrum of the 2D-CuI film is composed of two components, namely one component representing iodide species in direct contact with the metallic copper underneath and a second component that corresponds to the dominant emission of the covalently bound iodide in the 3D-CuI phase. The latter one has to be attributed to the terminating iodide species of the 2D-CuI film.

Interestingly, also the I4d emission originating from the 3D-CuI clusters (spectrum 3 in Fig. 15) has to be fitted with 2 components in order to reproduce the exact shape of the spin-orbit splitted signal. The chemical shifts here with $I4d_{5/2}$ peak maxima at E = 49.4 eV (component 1) and E = 49.89 eV (component 2) are almost identical to what we have found for the 2D-CuI film. The fact that also component 1 as the iodide species in direct contact to the metallic copper remains detectable even in the presence of the 3D-CuI clusters points to an inhomogeneous and rough surface morphology with coexisting 2D- and 3D-CuI-regions, in agreement with the impression given by Fig. 7f.

4. Conclusions

We have studied the oxidative CuI film formation on Cu(111) in an electrochemical environment by combined in situ STM and ex-situ SXPS measurements. We can summarize the results of the present study as follows:

(1) Iodide facilitates the copper oxidation due to the stabilization of cuprous species in form of CuI. Accordingly we observe a downward shift of the on-set potential of copper oxidation ($\Delta E \approx$ -160 mV) with respect to the pure supporting electrolyte (Fig. 1).

(2) Due to the insolubility of CuI we observe the formation of a CuI film on the electrode that inhibits the copper dissolution involving the net mass transport into solution. Consequently we observe an upward shift of the on-set of the dissolution reaction ($\Delta E \approx$ +60 mV) with respect to the pure supporting electrolyte (Fig. 1). The CuI iodide film, however, is a less effective passive layer than the Cu_2O/CuO, $Cu(OH)_2$ duplex film that can be grown on copper under alkaline conditions.

(3) The CuI film formation can be subdivided into an initial 2D-CuI film growth at lower potentials followed by the appearance of 3D-CuI clusters at higher potentials. The appearance of the 2D-CuI wetting layer on iodide modified copper surfaces could be understood as a thermodynamic effect.

(4) The 2D-CuI film is structurally related to the CuI(111) lattice of bulk CuI (zinc blende type). A Cu/I-bilayer thereby grows reversibly on-top of the pre-adsorbed iodide adsorbate layer whose electronic properties remain determined by the metal underneath.

References

1. P.C. Andricacos, C. Uzoh, J.O. Dukovic, J. Horkans, and H. Deligiani, *IBM J. Res. & Dev*., **42**, 567 (1998).
2. P.M. Vereecken, R.A. Binstead, H. Deligianni, and Andricacos, *P.C. IBM J. Res. & Dev*., **49**, 3 (2005).
3. T.P. Moffat, D. Wheeler, M.D. Edelstein, and D. Josell, *IBM J. Res. & Dev*., **49**, 19 (2005).
4. P. Broekmann, N.T.M. Hai, and K. Wandelt, *Surf. Sci*., **600**, 3971 (2006).
5. P. Broekmann, N.T.M. Hai, and K. Wandelt, *J. Appl. Electrochem*., **36**, 1241 (2006).
6. M. Wilms, M. Kruft, G. Bermes, and K. Wandelt, *Rev. Sci. Instr*., **70**, 3641 (1999).
7. T. Mayer, M.V. Lebedev, R. Hunger, and W. Jaegermann, *Applied Surf. Sci*., **252**, 31 (2005).
8. M. Wilms, P. Broekmann, C. Stuhlmann, and K. Wandelt, *Surf. Sci*., **416**, 121 (1998).
9. P. Broekmann, M. Wilms, and K. Wandelt, *Surf. Rev. Lett.*, **6**, 907 (1999).
10. P. Broekmann, M. Wilms, M. Kruft, C. Stuhlmann, and K. Wandelt, *J. Electroanal. Chem*., **467**, 307 (1999).
11. P. Broekmann, M. Wilms, M. Arenz, A. Spaenig, K. Wandelt in K. Wandelt, and S. Thurgate, (Eds.) "Solid LiquidInterfaces, Macroscopic Phenomena – Microscopic Understanding" *Topics in Applied Physics*, **85**, p.141, Springer (2003).
12. W.H. Li, J.H. Ye, S.F.Y. Li, and R.J. Nichols, *Surf. Sci*., **449**, 207 (2000).
13. M. Lennartz, M. Arenz, P. Broekmann, Ch. Stuhlmann, and K. Wandelt, *Surf. Sci*., **442**, 215 (1999).
14. M. Arenz, P. Broekmann, M. Lennartz, E. Vogler, and K. Wandelt, *Phys. Stat. Sol. A*, **187**, 63 (2001).
15. D.E. Irish, L. Stolberg, and D.W. Shoesmith, *Surf. Sci*., **158**, 238 (1985).
16. J. Inukai, Y. Osawa, and K. Itaya, *J. Phys. Chem. B*, **102**, 10034 (1998).
17. J. Kunze, V. Maurice, L.H. Klein, H.H. Strehblow, and P. Marcus, *J. Electroanal. Chem*., **554-555**, 113 (2003).
18. J. Kunze, V. Maurice, L.H. Klein, H.H. Strehblow, and P. Marcus, *Corr. Sci*., **46**, 245 (2004).
19. B. Obliers, P. Broekmann, and K. Wandelt, *J. Electroanal. Chem*., **554-555**, 183 (2003).
20. U. Bertocci, *Electrochim. Acta*, **11**, 1261 (1966).
21. B.V. Andryushechkin, K.N. Eltsov, and V.M. Shevlyuga, *Surf. Sci*., **566-568**, 203 (2004).